EM Implosion Memos

Memo 37

February 2010

Near-field time-of-arrival measurements for four feed-arms with a bicone switch

Prashanth Kumar, Serhat Altunc, Carl E. Baum, Christos G. Christodoulou and Edl Schamiloglu
University of New Mexico
Department of Electrical and Computer Engineering
Albuquerque, NM 87131

Abstract

This paper considers four feed-arms with a bicone switch. Spherical TEM waves are launched from the switch center and guided by the feed arms. Numerical simulations are used to examine the time-of-arrival of electric fields in the near field.

1 Introduction

The primary objective in the design of a switch system is to ensure that (approximate) spherical TEM waves originate from the switch center. The first stage in the design is to investigate the effects of the switch cone geometry.

Motivated by the prototype IRA (PIRA or IIRA), the initial approach assumed the center of the switch cones to be spatially isolated from the first focal point [1–4]. However, the results in [5] indicate that the geometric center of the cones can be shifted to coincide with the first focal point. This considerably simplifies the design and reduces the overall complexity of the switch system.

This paper examines two configurations, in which a bicone source, with its geometric center at the first focal point, is connected to the four feed arms of a PSIRA (or ΨRA). The first configuration consists of a *vertical* bicone source and the second consists of a *slanted* bicone source. A completely analytical treatment of the problem is too involved due to the complex geometry of the feed-arm and switch cone structures. Therefore, numerical simulations are used to obtain insight into the problem. Results examining the time of arrival of electric fields, in the near-field, are presented.

2 Determination of cone half-angles

The analytical relation between the impedance of a cone and its half-angle provides a starting point for the design of the switch cones. The half-angle and height are used to completely define the geometry of the cones. As a first approximation, the impedance of the cones is designed to match into the impedance of the feed arms of the PSIRA. The height of the cones is arbitrary, but the approximate dimensions in [6] are used.

2.1 Vertical switch cone

Consider the vertical switch cone geometry in Fig. 2.1. From [7], the pulse impedance of a circular cone antenna, over a ground plane, is given by

$$Z_c = \sqrt{\frac{\mu}{\epsilon}} \frac{1}{2\pi} \ln \left[\cot \left(\frac{\theta_0}{2} \right) \right], \tag{2.1}$$

where θ_0 is the half-angle of the cone. For a four feed-arm PSIRA, $Z_c = 100\ \Omega \Rightarrow \theta_0 = 21.37°$.

2.2 Slanted switch cone

For a given pulse impedance, Z_c', the half-angle of slanted circular cones, α, is determined using a stereographic projection. The stereographic projection formulas, Fig. 2.2, are detailed in [8] and are adopted for the switch cones shown in Fig. 2.3.

From Fig. 2.3, $\beta = (\pi/2) - \alpha$. The characteristic impedance for the bent circular cones is [8],

$$Z_c' = f_g Z_0, \tag{2.2}$$

where $Z_0 \approx 377\ \Omega$ is the impedance of free space. f_g is the geometric factor given by,

$$f_g = \frac{1}{\pi} \operatorname{arccosh} \left(\frac{\sin \beta}{\sin \alpha} \right). \tag{2.3}$$

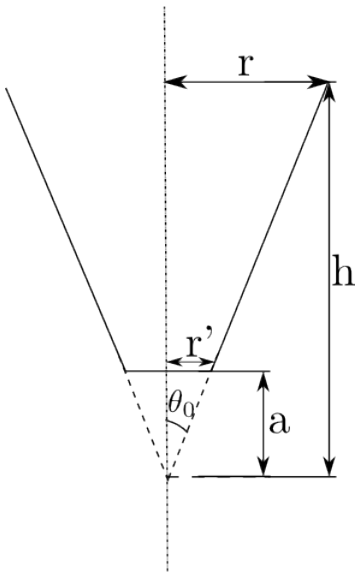

Figure 2.1: Diagram to calculate the half-angle of a vertical switch cone for a given pulse impedance.

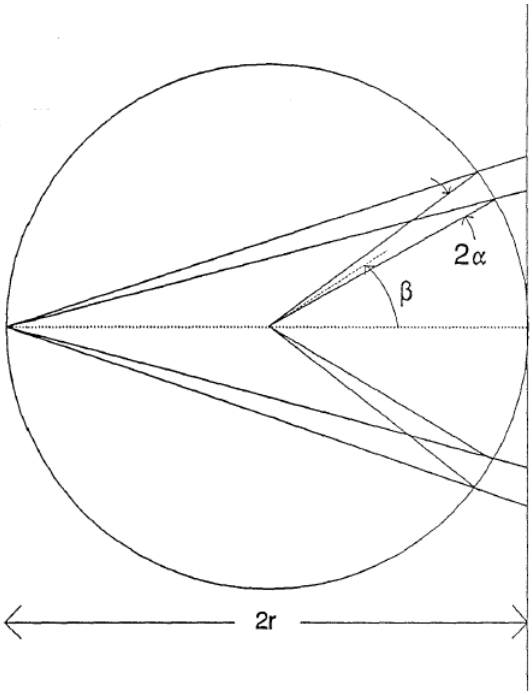

Figure 2.2: Stereographic projection to determine the half-angle of bent circular cones [8].

For the four feed-arm PSIRA, $Z_c' = 200\ \Omega$[1]. The half-angle is,

$$\alpha = \text{arccot}\left[\cosh\left(\pi\frac{Z_c'}{Z_0}\right)\right] = 20.04^\circ, \tag{2.4}$$

which is less than the half-angle for the vertical switch cones.

[1]note that equation (2.2) is for a bicone whereas equation (2.1) is for a single cone over a ground plane

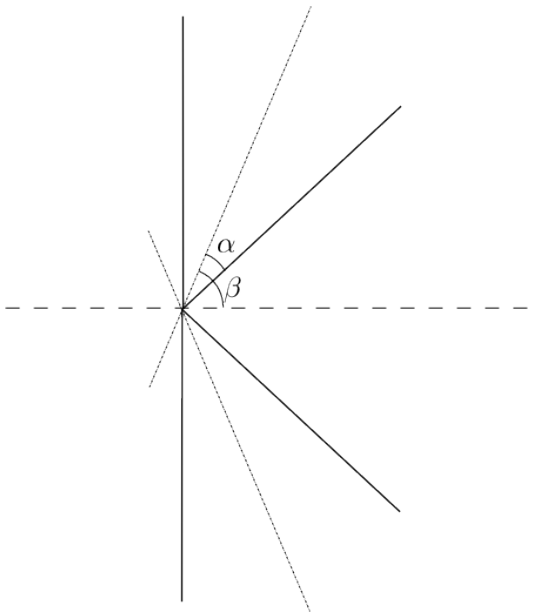

Figure 2.3: Diagram to calculate the half-angle of a slanted switch cone for a given pulse impedance.

3 Simulation setup

3.1 Structure visualization

3.1.1 Four feed arms with vertical switch cones

The perspective, front and side views of the vertical switch cones, connected to the feed arms, are shown in Fig. 3.1.

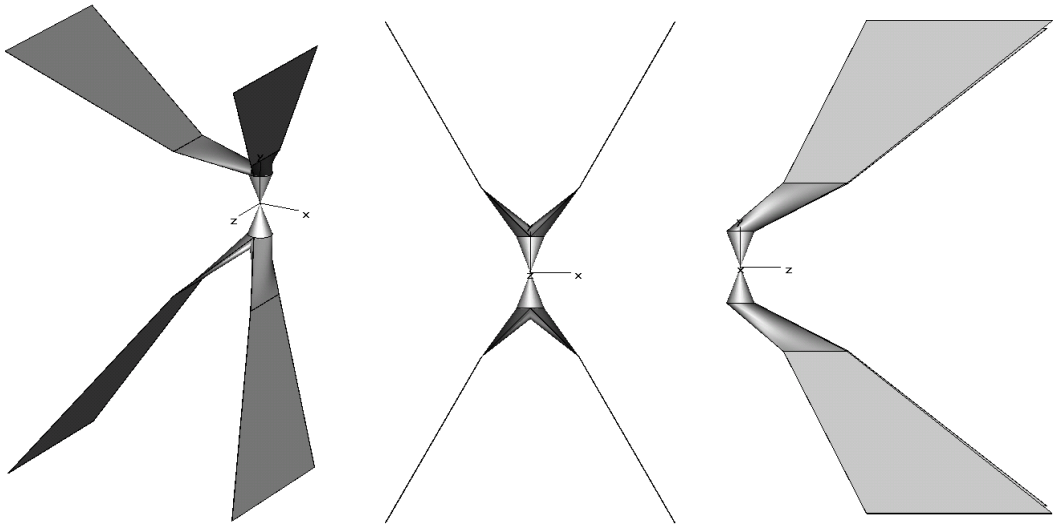

(a) Perspective view (b) Front view (c) Side view

Figure 3.1: Perspective, front and side views of the vertical bicone switch and four feed-arm system.

The bicone impedance is 200 Ω, to match into the impedance of the feed arms. The geometric center of the switch cones is the first focal point. The connection between the circular base of the switch cones and the flat face of the feed-arms will henceforth be referred to as the "loft" connection, in accordance with terminology used by CST®Microwave Studio, as shown in Fig. 3.2. The details of the switch cone geometry and excitation are shown in Fig. 3.3.

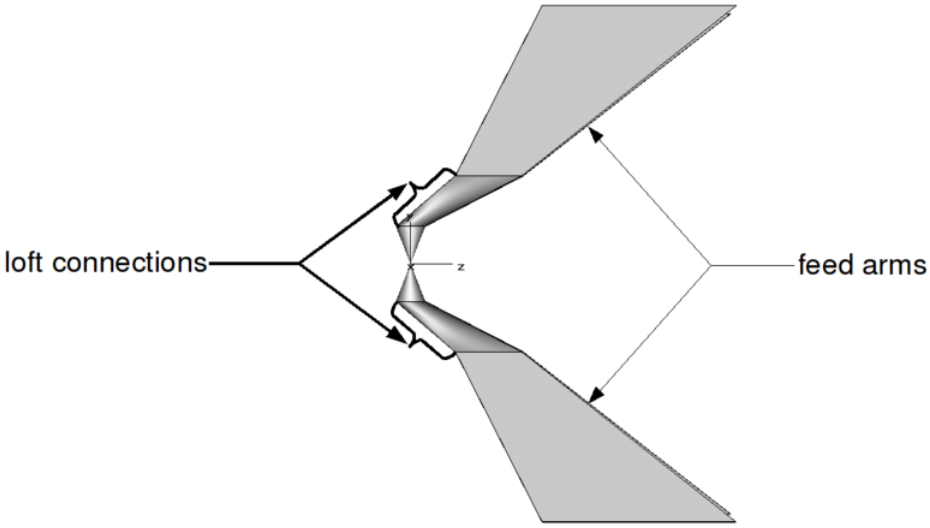

Figure 3.2: "Loft" connection between circular switch cone base and feed arms.

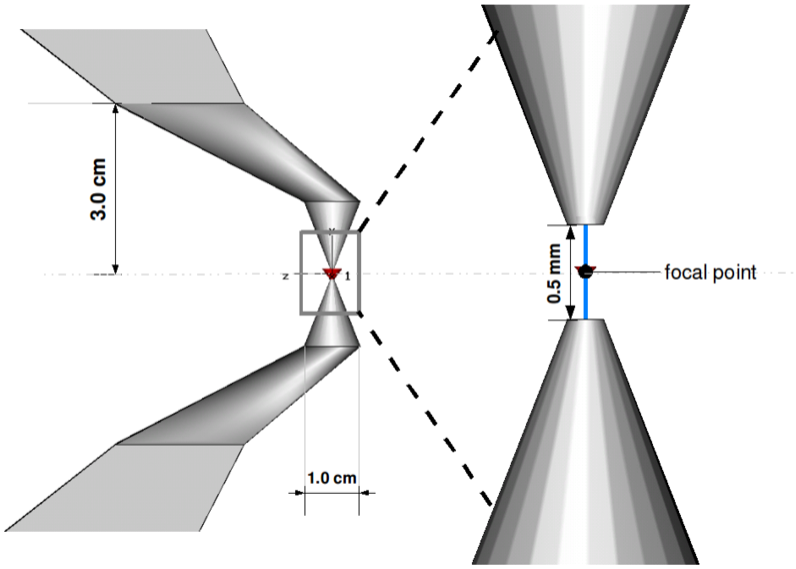

Figure 3.3: Geometric details of the switch cones and loft connections. The geometric center of the switch cones is located at the first focal point. The excitation is applied between a 0.5 mm gap.

3.1.2 Four feed arms with slanted switch cones

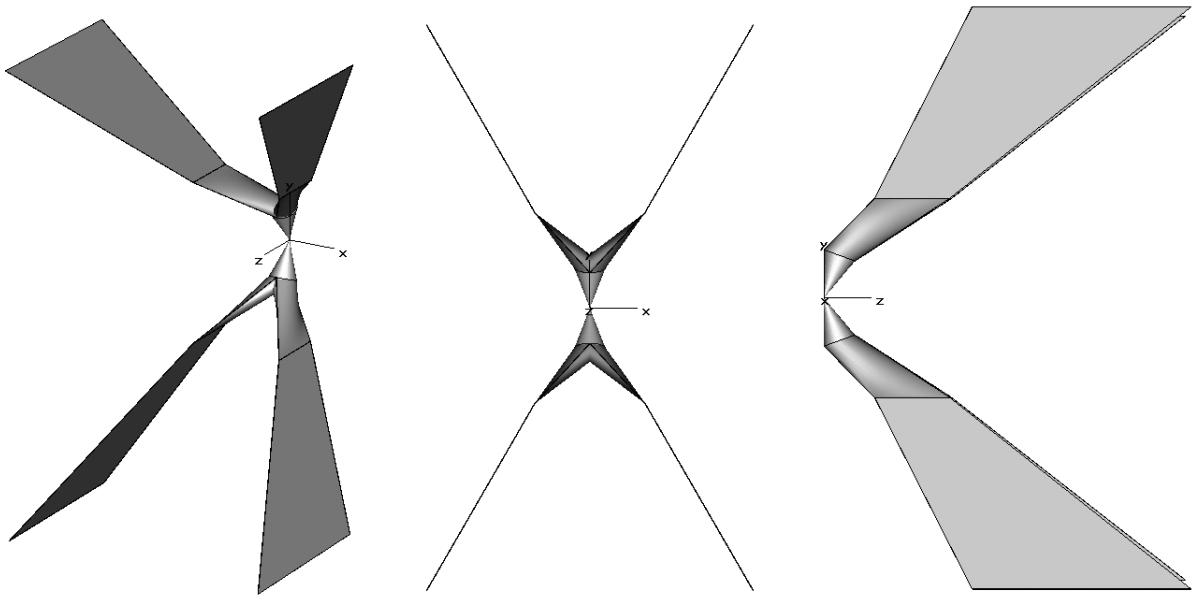

(a) Perspective view (b) Front view (c) Side view

Figure 3.4: Perspective, front and side views of the slanted bicone switch and four feed-arm system.

The perspective, front and side views of the slanted switch cones, connected to the feed arms, are shown in Fig. 3.4. The radius of the cones and the loft length are identical to Fig. 3.3. Each switch cone has an impedance of 100 Ω to match into the impedance of the feed-arms. The (virtual) apex of the cones meet at the first focal point.

3.2 Excitation

A 25 ps, 1 V, ramp rising step excitation was applied between a 0.5 mm gap. For the vertical cones, the discrete port excitation passes through the focal point as shown in Fig. 3.3. For the slanted cones, this is not the case (although the distance between the discrete port and focal point is less than ≈ 0.12 mm).

3.3 Electric field probe placements and orientations

It is desired to observe the time of arrival of the electric fields in the near-field. Therefore, electric field probes were placed on a (virtual) sphere of radius 3.0 cm centered at the first focal point. Three probes, oriented along the x, y and z direction, were placed at every point. The probes were placed on the xy, $-yz$ and $-zx$ planes, i.e., in the direction of propagation *toward* the reflector as shown in Fig. 3.5. The labeling conventions adopted are shown in Fig. 3.6.

The (x, y, z) components of the electric fields, obtained from the probes, were converted into the equivalent (r, θ, ϕ) components to obtain the tangential and normal components on the (virtual)

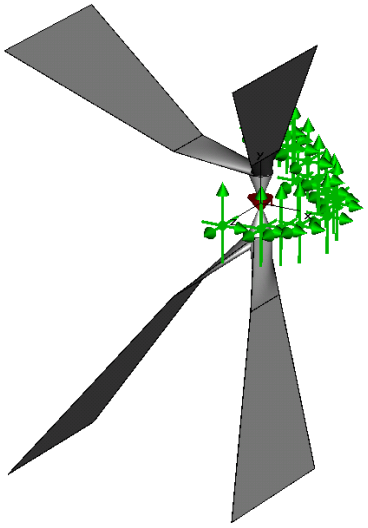

Figure 3.5: Perspective view of probe locations.

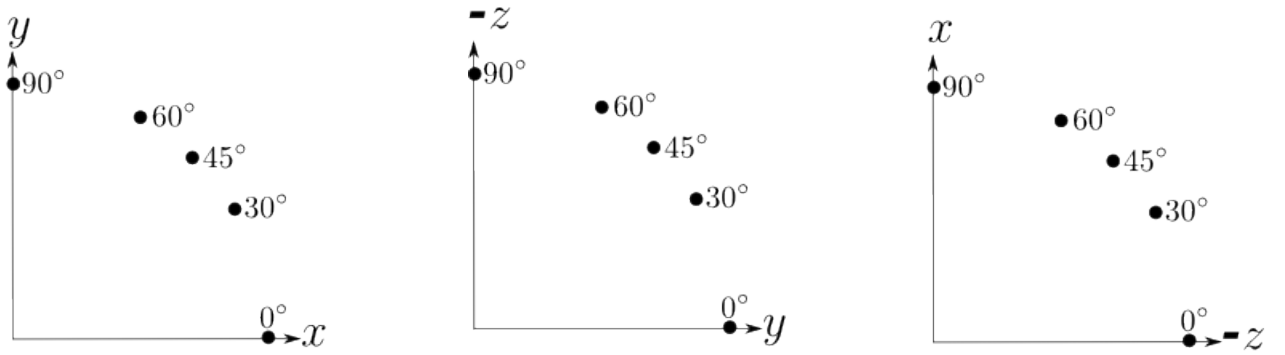

(a) Probe placements in the xy plane

(b) Probe placements in the $-yz$ plane

(c) Probe placements in the $-zx$ plane

Figure 3.6: Labeling conventions for the electric field probe placements in the xy, $-yz$ and $-zx$ planes.

measurement sphere. The conventional definition of the spherical coordinate system, Fig. 3.7[2], was used, i.e.,

$$E_r = E_x \sin\theta\cos\phi + E_y \sin\theta\sin\phi + E_z\cos\theta \tag{3.1}$$

$$E_\theta = E_x \cos\theta\cos\phi + E_y \cos\theta\sin\phi - E_z\sin\theta \tag{3.2}$$

$$E_\phi = -E_x \sin\phi + E_y\cos\phi \tag{3.3}$$

[2]Figure excerpted from Balanis, Advanced Engineering Electromagnetics

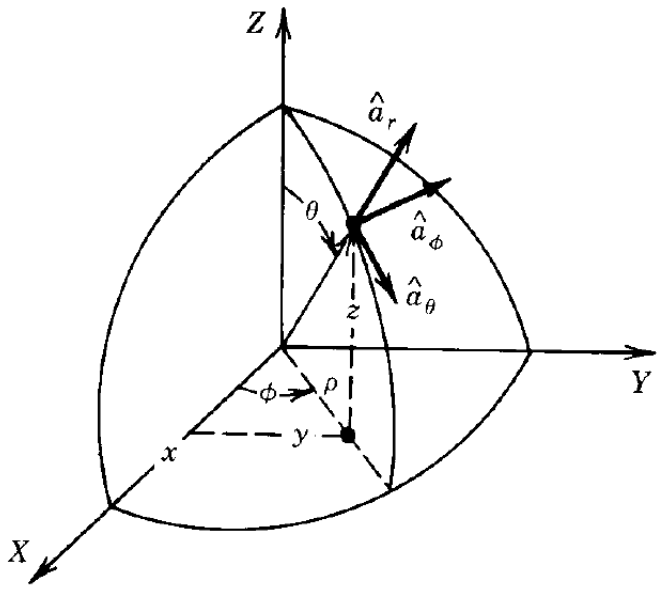

Figure 3.7: Conventional cartesian↔spherical coordinate system

3.4 Important CST parameters

Domain	Time
Excitation	Discrete
Input	Ramp rising with 25 ps rise time
Excitation voltage	1 V
Frequency range	0−40 GHz
LPW	10

3.5 Discussion

Since we are only interested in the near-field region, i.e., around the switch cones, the simulation space can be considerably reduced, allowing for increased numerical resolution. Hence, the feed arms are truncated in the setups shown in Fig. 3.1 and Fig. 3.4.

The calculations of the cone half-angles in section 2 only serve as a first approximation in the design. This is because the (arbitrary) loft connections complicate the problem. For a probe at some fixed location in the near field, there may be alternate ray paths within the rise time of the input pulse that would contribute to the electric field as shown in Fig. 3.8. If a spherical wave emanates from the first focal point, the electric fields should arrive on all the near-field probes at exactly the same time.

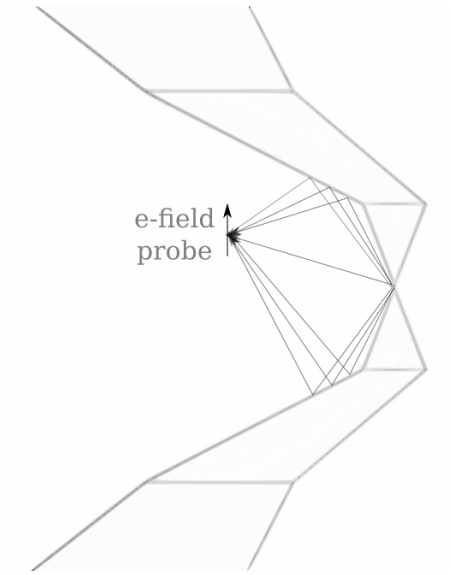

Figure 3.8: Alternate ray paths within the rise time, t_δ, that contribute to the electric field on a probe located in the near field.

4 Results

4.1 Four feed arms with vertical switch cones

The normalized E_θ and E_ϕ components of the electric field responses in the xy, $-yz$ and $-zx$ planes are shown in Fig. 4.1 (in each figure, every curve is normalized with respect to its maximum). The normalized results provide a comparitive insight into the time of arrival of the electric fields (clear times) on the same plane. The E_ϕ component in the $-yz$-plane and the E_θ component in the $-zx$-plane should be zero, as observed in Fig. 4.1(c) and Fig. 4.1(f). The $-zx$ plane contains only the normalized E_y component and as observed in Fig. 4.1(e), the time spread is less than 2 ps in this plane. As seen in Fig. 4.1(a) and Fig. 4.1(d), the normalized E_ϕ component in the $xy-$plane and the normalized E_θ component in the $-yz$-plane show a spread of less than 5 ps. The largest deviations, of the order of $\approx$10-20 ps, are observed in the normalized E_θ component in the xy-plane, Fig. 4.1(b). However, by symmetry, for every E_θ component there exists an equal and opposite E_θ component. These equal and opposite components cancel each other and do not contribute toward the impulse response at the second focal point.

4.2 Four feed arms with slanted switch cones

The results are almost identical to the vertical switch cones in Fig. 4.1. The oscillations in late time for some responses is most likely due to numerical errors in the simulation. The only noticable difference is in the normalized E_θ component in the $xy-$plane, as seen in Fig. 4.2(b). This component has a smaller time spread, less than 10 ps, for approximately 30 ps (t_δ) after which the time spread between the curves increases. The better agreement, compared to the vertical bicone switch, is most likely due to the smoother transition of the loft connections.

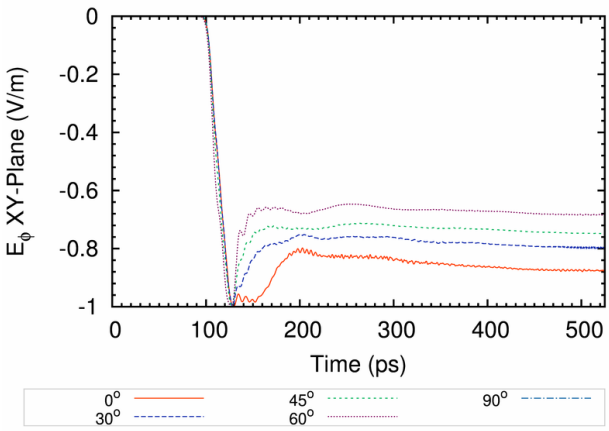

(a) Normalized E_ϕ in the $xy-$plane

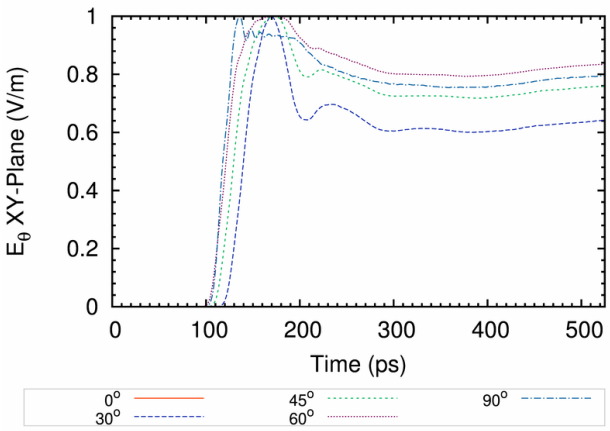

(b) Normalized E_θ in the $xy-$plane

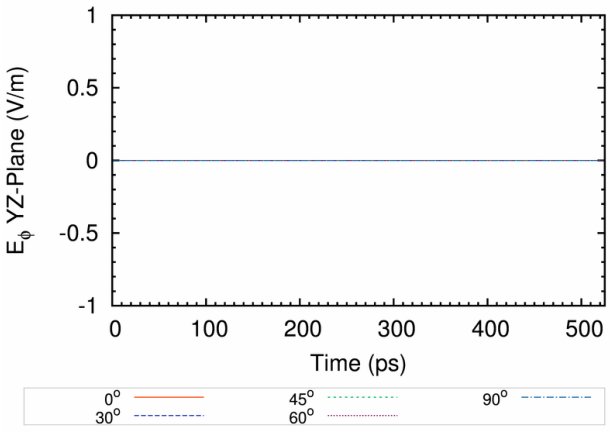

(c) Normalized E_ϕ in the -$yz-$plane

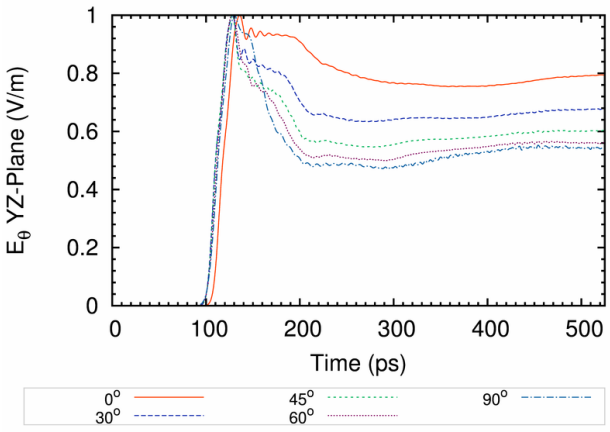

(d) Normalized E_θ in the -$yz-$plane

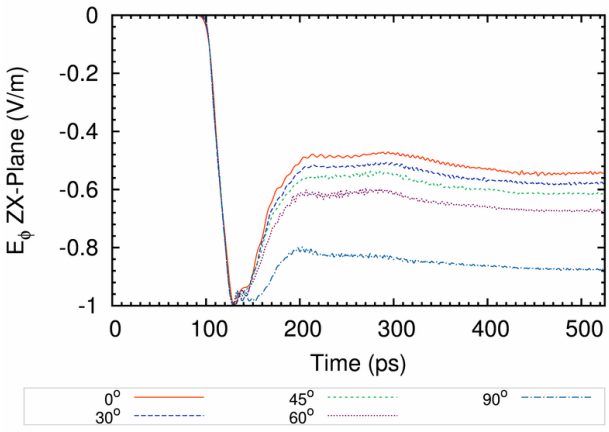

(e) Normalized E_ϕ in the -$zx-$plane

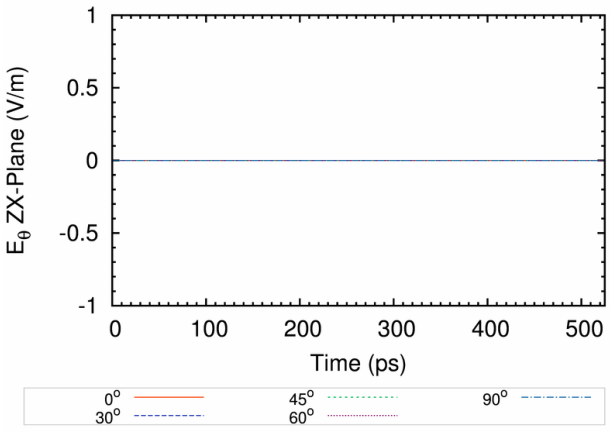

(f) Normalized E_θ in the -zxplane

Figure 4.1: Normalized E_θ and E_ϕ components of the responses from the electric field probes on the $xy, -yz$ and $-zx$ planes for the vertical bicone switch configuration.

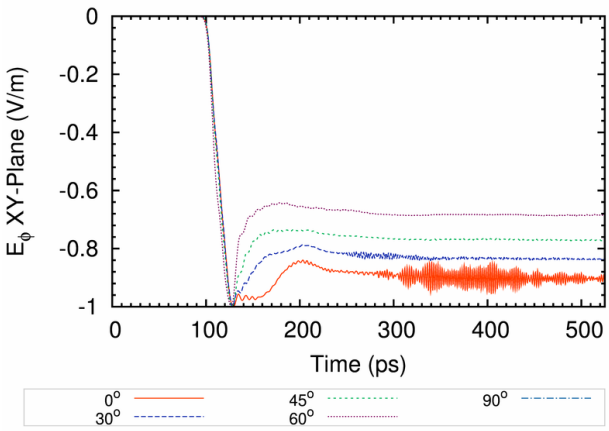

(a) Normalized E_ϕ in the $xy-$plane

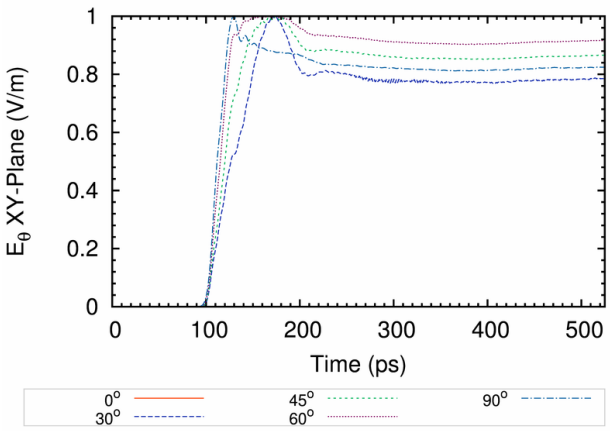

(b) Normalized E_θ in the $xy-$plane

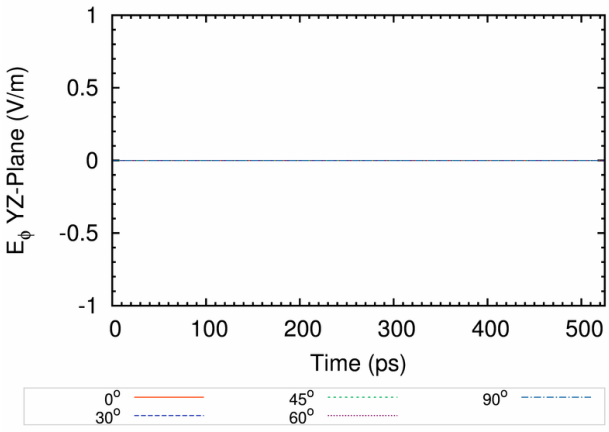

(c) Normalized E_ϕ in the -$yz-$plane

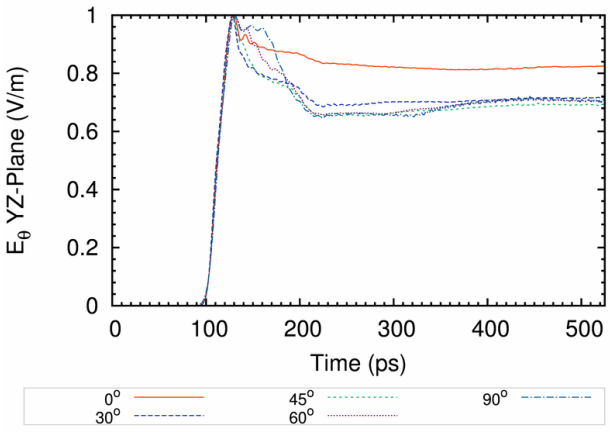

(d) Normalized E_θ in the -$yz-$plane

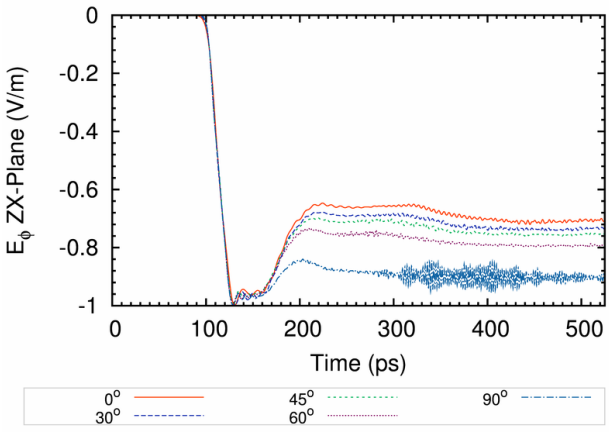

(e) Normalized E_ϕ in the -$zx-$plane

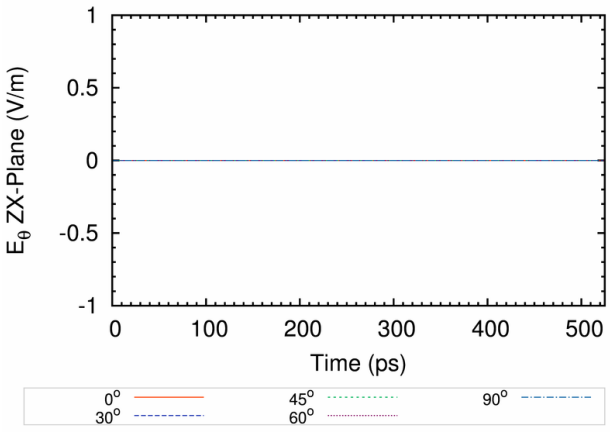

(f) Normalized E_θ in the -zxplane

Figure 4.2: Normalized E_θ and E_ϕ components of the responses from the electric field probes on the $xy, -yz$ and $-zx$ planes for the slanted bicone switch configuration.

4.3 The affect of the setup geometry on the electric field

Specific features pertaining to the geometry of the simulation setup can be identified from the electric field responses in Fig. 4.1 and Fig. 4.2. Figure 4.3 illustrates this point using Fig. 4.1(e) as an example. The initial rise, $t_\delta = 25$ ps, represents propagation of the spherically expanding wave along the, rotationally symmetric, switch cones. Good agreement in the electric field responses is observed up to the height of the cones, i.e., 1.27 cm $\approx$ 40 ps. The deviation observed after $\approx$ 40 ps represents the propagation of the wave along the feed arms, which is more non-uniform due to the lack of rotational symmetry.

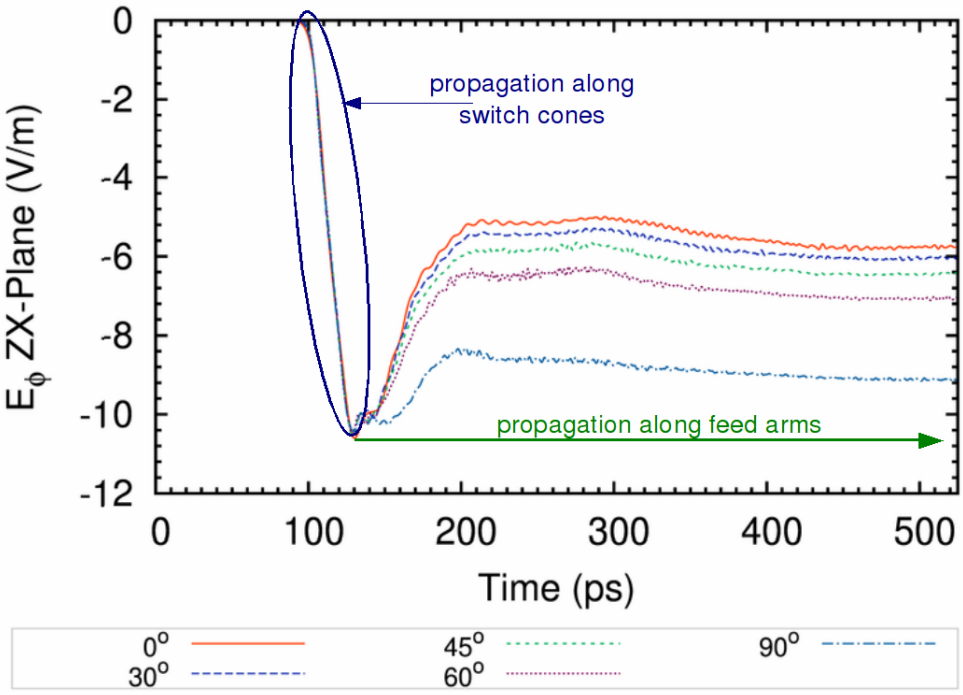

Figure 4.3: Features observed in the electric field probe responses using the E_ϕ component in the $zx-$plane as an example.

5 Conclusions

The spherical components of the normalized electric fields in the $xy, -yz$ and $-zx$ planes are identical, at least in early time (time of interest), for both the vertical and slanted switch cone cases. The normalized E_θ component in the $xy-$plane for the slanted bicone switch shows a smaller time spread compared to the corresponding result for the vertical bicone switch.

The observations regarding the geometry of the simulation setup in Section 4.3 give rise to an interesting possibility. Switch cones, of appropriate height, can be used to guide the spherically expanding TEM waves thus eliminating the need of the feed arms. The switch cones can therefore act as both the source and the guide, making the geometry of the switch region much simpler. Such a rotationally symmetric bicone configuration would also ensure the field remains uniform in the time of interest, t_δ. Such a design warrants further investigation.

References

[1] Prashanth Kumar, Carl E. Baum, Serhat Altunc, Christos G. Christodoulou and Edl Schamiloglu . Analytical considerations for curve defining boundary of a non-uniform launching lens. EM Implosion Memo 26, June 2009.

[2] Prashanth Kumar, Carl E. Baum, Serhat Altunc, Christos G. Christodoulou and Edl Schamiloglu . Simulation results for 3-layer and 6-layer planar non-uniform launching lens. EM Implosion Memo 27, June 2009.

[3] Prashanth Kumar, Carl E. Baum, Serhat Altunc, Christos G. Christodoulou and Edl Schamiloglu . Derivation of the dielectric constant as a function of angle for designing a conical non-uniform launching lens. EM Implosion Memo 28, June 2009.

[4] Prashanth Kumar, Carl E. Baum, Serhat Altunc, Christos G. Christodoulou and Edl Schamiloglu . Simulation results for 6-layer and 7-layer conical non-uniform launching lens. EM Implosion Memo 29, June 2009.

[5] Prashanth Kumar, Carl E. Baum, Serhat Altunc, Christos G. Christodoulou and Edl Schamiloglu . Design and numerical simulation of switch and pressure vessel setup - part II. EM Implosion Memo 32, August 2009.

[6] Prashanth Kumar, Carl E. Baum, Serhat Altunc, Christos G. Christodoulou and Edl Schamiloglu . Design and numerical simulation of switch and pressure vessel setup - part I. EM Implosion Memo 31, August 2009.

[7] Carl E. Baum. A Circular Conical Antenna Simulator. Sensor and Simulation Note 36, March 1967.

[8] E. G. Farr and C. E. Baum. Prepulse Associated with the TEM Feed of an Impulse Radiating Antenna. Sensor and Simulation Note 337, March 1992.